Progress of Quantum Hall Research for Disseminating the Redefined SI

Albert F. Rigosi, Mattias Kruskopf, Alireza R. Panna, Shamith U. Payagala, Dean G. Jarrett, Randolph E. Elmquist, and David B. Newell

Uncorrected Proof

Contents

A. F. Rigosi (✉) · A. R. Panna · S. U. Payagala · D. G. Jarrett · R. E. Elmquist · D. B. Newell
Physical Measurement Laboratory, National Institute of Standards and Technology, Gaithersburg, MD, USA
e-mail: albert.rigosi@nist.gov; Alireza.Panna@nist.gov; shamith.payagala@nist.gov; dean.jarrett@nist.gov; randolph.elmquist@nist.gov; david.newell@nist.gov

M. Kruskopf
AU1 Electricity Division, Physikalisch-Technische Bundesanstalt, Brunswick, Germany
e-mail: mattias.kruskopf@ptb.de

© Springer Nature Singapore Pte Ltd. 2022

D. K. Aswal et al. (eds.), *Handbook of Metrology and Applications*,
https://doi.org/10.1007/978-981-19-1550-5_17-1

TRIAL MODE - Click here for more information

Historical Context

AU2
AU3

Basics of the Quantum Hall Effect

To fully appreciate the impacts that the discovery of the quantum Hall effect (QHE) had on electrical metrology, it may benefit the reader to cultivate a general understanding of the phenomenon (Von Klitzing and Ebert 1985; Von Klitzing et al. 1980). For the purposes of this handbook, a basic overview will be given. The QHE may be exhibited by a two-dimensional (2D) electron system when placed under a strong magnetic field perpendicular to the plane of the system. These conditions lead to quantization, or discrete energy states for charged particles in the magnetic field. These energy values, determined by solving the Schrödinger equation, are known as Landau levels. In precise measurements, one defines the quantized Hall resistance R_{xy} as the measured voltage, perpendicular to the direction of the applied current, divided by that same current. The characteristic longitudinal resistivity ρ_{xx} goes to zero as R_{xy} approaches a quantized value over a range of magnetic field strength (nominally, a QHE plateau).

Since the discovery of the QHE at the start of the 1980s, the electrical metrology community has sought to implement a resistance standard based on the theoretical relation: $R_{\mathrm{H}}(\nu) = R_{xy}(\nu) = h/\nu e^2$, where ν is an integer related to the Landau energy level, and h and e are the Planck constant and elementary charge, respectively. In 1990 the QHE was assigned a conventional value as an empirical standard based on the determination of fundamental constants through experiments such as the calculable capacitor, which uses the Thompson-Lampard theorem (Thompson and Lampard 1956) to experimentally realize the unit of impedance, the farad, as defined by the International System of Units (SI). When the redefinition of the SI occurred in 2019, the constants h and e were assigned globally agreed-upon exact SI values such that the electrical units of the ohm, volt, and ampere are defined by relation to these fundamental constants. Interestingly, the electrical quantum standards of resistance and voltage now realize the SI unit of mass, the kilogram, through the exact value of h and an experiment called the Kibble Balance (Kibble 1976; Schlamminger and Haddad 2019). Within the redefined SI, many other fundamental constants are exact or have greatly reduced uncertainties (Tiesinga et al. 2021). For instance, the von Klitzing constant is now exact, calculated from h/e^2 ($R_{\mathrm{K}} = 25\ 812.807\ 45\ldots\ \Omega$).

Before the QHE, resistance metrologists would employ standard resistors made from copper-manganese-nickel and similar stable alloys. These standards behaved differently in locations around the world due to variation of their nominal resistance (Witt 1998), and this robust, time-independant definition based on the ratio of fundamental constants has developed to allow expansion of the focus of the field.

Predecessors for Quantum Hall Standards

Quantum Hall standards began their journey shortly after the QHE was discovered. Some of the earliest devices were based on silicon metal–oxide–semiconductor field-effect transistors (MOSFETs). For Si systems, the electric field needed to define the

Uncorrected Proof

TRIAL MODE - Click here for more information

energy state of electrons in two dimensions was generated by a planar metallic voltage gate separated from the surface of the semiconductor by an insulating oxide layer. In work performed by Hartland et al., a cryogenic current-comparator (CCC) bridge with a precise 1:1- or 2:1-ratio was used to compare two quantized Hall resistances, one from the MOSFET and the other from a gallium arsenide (GaAs) heterostructure, which employs layers of semiconductors to create a 2D quantum well (Hartland et al. 1991). Both QHE devices were operated at the same temperature and magnetic field, but on different Landau levels. The critical components of the CCC were immersed in liquid helium at 4.2 K and were shielded from external magnetic fields using superconducting lead foil and low-temperature ferromagnetic alloy (Hartland et al. 1991).

This work focused on comparing the quantized Hall resistance (QHR) of the GaAs/AlGaAs heterostructure (measured at the $\nu = 2$ plateau, or $h/2e^2$, which is approximately 12.9 kΩ) to that of the silicon MOSFET device (measured at the $\nu = 4$ plateau, or $h/4e^2$, about 6.45 kΩ). The deviations from the expected ratio of 2:1, summarized in Fig. 1, are represented as Δ_{24} and the ratio of the winding ratio allows two resistances to be compared while canceling out the multiplicative factor of 2 between them. These results suggest that the two QHR values agree within 2 $[1 - 0.22(3.5) \times 10^{-10}]$, where the uncertainty is in parentheses. Given the novelty of the QHE at the time, this type of experiment was effective in supporting the notion of representing the plateaus as based on the fundamental constants.

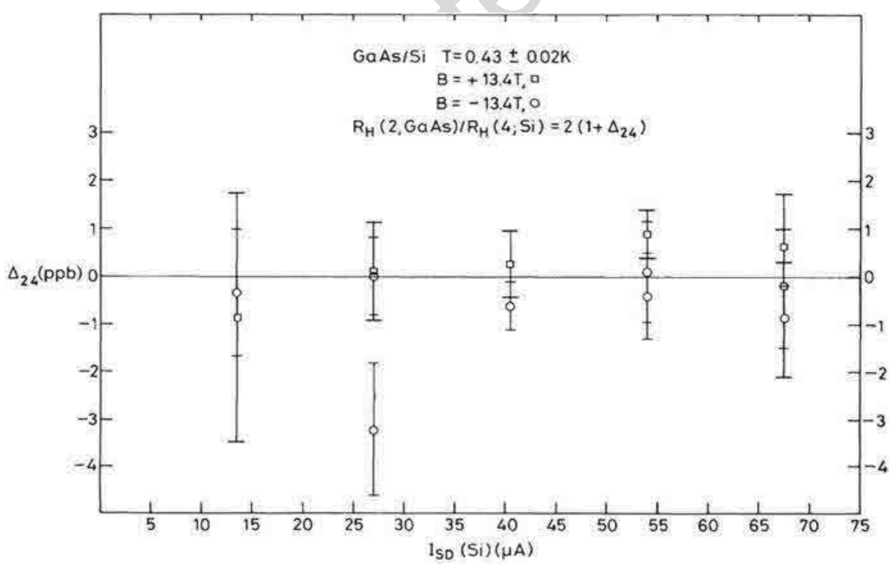

Fig. 1 Measurements of Δ_{24} expressed in parts per billion (ppb, or nΩ/Ω) for the direct comparison of the GaAs-based device (at the $\nu = 2$ plateau) and the Si MOSFET device (at the $\nu = 4$ plateau). These data are shown as a function of the applied current through the Si MOSFET device, and the error bars represent a 1σ random error of the average of Δ_{24}. (Reprinted figure with permission from (Hartland et al. 1991). Copyright 1990 by the American Physical Society)

TRIAL MODE - Click here for more information

One of the disadvantages of MOSFETs was the high magnetic field required during an experiment. Laboratory magnetic fields of the time typically yielded a resistance plateau that was only quantized over a narrow range of magnetic field. As seen in (Hartland et al. 1991), the Si MOSFET device required 13 T to access its $\nu =$ 4 plateau, and currents above 10 μA would cause the QHE to break down, or lose its precise quantized value. These devices did not stay long in favor since GaAs-based devices quickly demonstrated more optimal behavior (Cage et al. 1985; Hartland 1992). In GaAs-based devices, a 2D layer of electrons forms when an electric field forces electrons to the interface between two semiconductor layers (the other, in this case, being AlGaAs). For many devices with this type of interface, the layers were grown via molecular beam epitaxy (Tsui and Gossard 1981; Hartland et al. 1985). Similar heterostructures were developed in InGaAs/InP, which were obtained via metal-organic chemical vapor deposition (Delahaye et al. 1986).

These early GaAs-GaAlAs heterostructure devices were grown with excellent homogeneity and exhibited high mobilities (on the order of 200 000 $cm^2V^{-1}s^{-1}$) at 4 K. The success of this material in providing highly precise quantized resistances led in 1990 to the definition of the $R_{K\text{-}90}$ representation of the ohm as recommended by the Consultative Committee for Electricity (CCE) (Taylor 1990). For another 20 years, technologies continued to improve, allowing both GaAs-based resistance standards and cryogenic measurement methods to offer increased sensitivity and precision (Jeckelmann et al. 1997; Williams 2011).

During the 1980s, metrologists at national metrology institutes (NMIs) utilized these high-quality devices to confirm the universality of the von Klitzing constant R_K over the course of many experiments. An example of the use of GaAs-based devices for metrology can be seen in Cage et al. (1985), where the authors looked to adopt GaAs as a standard used to maintain a laboratory unit of resistance. The work again demonstrated the universality of the QHE and showed the viability of the device as a means to calibrate artifact standards. The devices were grown by molecular beam epitaxy at an AT&T Bell Laboratory facility in New Jersey (Cage et al. 1985) and had dimensions as shown in the inset of Fig. 2. The magnetic field sweep data for the Hall and longitudinal voltages are also shown in Fig. 2a. The second part of the experiment involved transferring the QHE value through 1:1 comparisons to a set of 6453.2 Ω resistors, and from there to the US ohm, maintained with a group of resistors at the 1 Ω level (Hamon 1954). Comparisons were done using a direct current comparator (DCC) resistance bridge and reconfigurable series-parallel resistor networks at several resistance levels (Cage et al. 1985).

Before a QHR device can be utilized for calibration, it needs to pass a characterization procedure. The main purpose here is to identify instabilities over time as well as asymmetries in the device properties for different combinations of contacts. The systematic series of CCC measurements shown in Fig. 2b involves various combinations of orthogonally and diagonally aligned pairs of Hall contacts inside the device. It is performed at the same fixed *B*-field intended to be later used for the calibration procedure in which the QHR will be the reference. The suitable *B*-field, where the deviation from $R_K/2$ is expected to be on the level of 1 nΩ/Ω, is typically identified prior to this procedure by characterizing the longitudinal resistivity ρ_{xx} at several points within the resistance plateau.

Uncorrected Proof

TRIAL MODE - Click here for more information

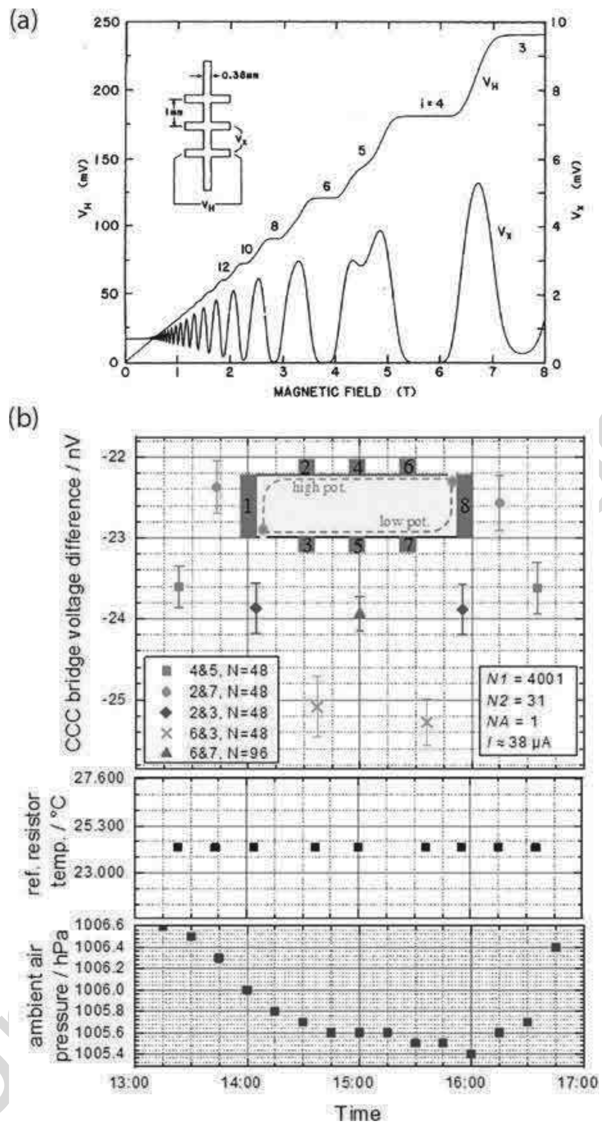

Fig. 2 (**a**) Hall and longitudinal voltage measurements from a magnetic field sweep of a GaAs-based device. The temperature was 1.2 K and the applied current was 25.5 μA. © 1985 IEEE. Reprinted, with permission, from (Cage et al. 1985). (**b**) A practical example of the final high accuracy device characterization procedure prior to calibration at a fixed *B*-field where the deviation from $R_K/2$ is expected to be below 1 nΩ/Ω. The characterization procedure of the device (CCC bridge voltage difference) involves a series of CCC measurements at diagonally and orthogonally aligned Hall contact pairs with the primary purpose of identifying instabilities over time as well as asymmetries in the device properties. The quantity *N* describes the number of measurement cycles in the CCC measurement. The error bars represent type A expanded measurement uncertainties ($k = 2$). To identify instabilities related to the room-temperature reference resistor, the ambient air pressure and the reference resistor temperature are recorded simultaneously as one characterizes the QHR device

TRIAL MODE - Click here for more information

A series of eight symmetrically arranged Hall measurements at five pairs of Hall contacts (see inset in Fig. 2b) are applied in the following order: (1) contacts 4 and 5, (2) contacts 2 and 7, (3) contacts 2 and 3, (4) contacts 6 and 3, (5) contacts 6 and 7, (6) contacts 2 and 3, (7) contacts 2 and 7, (8) contacts 4 and 5. Whereas the contact pairs 2 and 7 (and 6 and 3) are diagonally aligned and thus have a longitudinal resistance component, the other contact pairs 4 and 5, 2 and 3, and 6 and 7 are orthogonally aligned Hall contacts. Therefore, in the case where a device exhibits equal quantization in all regions, the Hall resistances and corresponding bridge voltages at the Hall contact pairs 4 and 5, 2 and 3, and 6 and 7 should be the same within the expanded uncertainties. Since the remaining contact pairs 2 and 7 (and 6 and 3) have a longitudinal component across the full accessible length of the device, they should deviate from the previous three pairs according to their longitudinal resistance component. The results of the practical example, plotted in Fig. 2b, represent a typical pattern of such a measurement series. The difference voltage in nV represents average data derived using a CCC in a series of current-reversed measurements. The measured bridge voltage difference can be used to calculate the value of the unknown resistor if the reference resistor value, winding ratio, and compensation network configuration are known quantities (Götz et al. 2009).

In the case of instabilities in the QHR device or the reference resistor, the measurement results can be asymmetrically distributed or not be reproducible over time within the expanded uncertainties. Additionally, the noise and uncertainty figures of the individual measurements should be similar for all pairs of contacts. A typical expanded ($k = 2$) type A uncertainty of a CCC bridge voltage in a QHR versus a 100 Ω measurement is below 0.5 nV after 48 measurement cycles. To be able to identify instabilities caused by the reference resistor, it is recommended to simultaneously record the ambient pressure and resistor temperature during the measurement as shown in the bottom panels of Fig. 2b. The final dc calibration procedure in which the QHR is used as a reference is typically realized by using the center Hall contact pair 4 and 5.

Expansion of QHR Device Capabilities

QHR devices soon became the norm in the electrical metrology community, with many of the NMI efforts implementing the new standards based on GaAs devices (Small et al. 1989; Cage et al. 1989; Delahaye and Jeckelmann 2003; Jeckelmann and Jeanneret 2001). Compared to the part-per-million or larger changes that occurred over the years before 1990 in many NMI ohm representations based on standard resistors, better agreement was obtained (by an order of magnitude) between the various worldwide NMIs in later resistance intercomparisons. However, to calibrate standards at resistance levels far removed from the QHR value, several stages of resistance ratio scaling were required and the uncertainty increased with each stage. The next natural step for metrologists was to examine whether or not these QHR devices could accommodate other values of resistance so that the calibration chain could be shortened. More advanced experiments and models

Uncorrected Proof

TRIAL MODE - Click here for more information

were developed by studies of QHE behavior and showed how this may be accomplished by constructing quantum Hall array resistance standards (QHARS) (Oe et al. 2013; Poirier et al. 2004; Ortolano et al. 2014; Konemann et al. 2011).

For instance, in Oe et al., a 10 kΩ QHARS device was designed and consisted of 16 Hall bars, providing a more easily accessible decade resistance value compared to previous work (Oe et al. 2013). The nominal value of the device was about 34 nΩ/Ω from 10 kΩ (based on R_{K-90}). The design and final device can be seen in Fig. 3. The device was measured using a CCC to compare the device against an artifact calibrated using another well-characterized QHR device. In this case, a 100 Ω standard resistor was used to verify that the array device agreed with its nominal value to within approximately one part in 10^8. The work also proposed new combinations of Hall bars such that the array output could be customized for any of the decade values between 100 Ω and 1 MΩ (Oe et al. 2013).

In addition to the benefits gained from expanding GaAs-based devices further into the world of metrology using direct current (DC), expansion was also explored in the realm of alternating current (AC). Various NMIs began standardizing impedance by using the QHE in an effort to replace the calculable capacitor, which is a difficult apparatus to construct and time-consuming to operate (Ahlers et al. 2009; Cabiati et al. 1999; Bykov et al. 2005; Hartland et al. 1995; Wood et al. 1997). The QHE still exhibited plateaus even at very high excitation frequencies, as shown in Bykov et al., which described the behavior of the 2D electron system in GaAs-based devices for frequencies between 10 KHz and 20 GHz (Bykov et al. 2005). However, when the applied current was AC, a new set of oscillations dependent on the

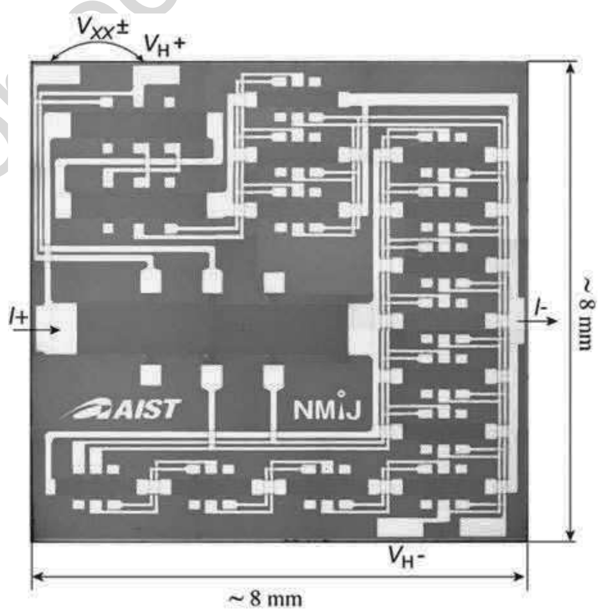

Fig. 3 A 10 kΩ QHARS device is shown with 16 Hall bars. The chip has lateral dimensions of 8 mm per side and was fabricated to be mounted on a standard transistor outline (TO)-8 package. The contact pads are labeled based on whether they are used for current injection or voltage measurements. (© 2013 IEEE. Reprinted, with permission, from (Oe et al. 2013))

Uncorrected Proof

TRIAL MODE - Click here for more information

magnetic field was found. This is relevant for impedance metrology because having a longitudinal resistance very close to zero is one mark of a well-quantized device, and having AC frequency-dependent oscillations would undoubtedly increase the uncertainty associated with the QHR. Challenges in adopting QHR technology still exist today in this branch of electrical metrology.

The Graphene Era Begins

Comparing Graphene to GaAs

At the end of the 2000s, research in 2D materials like graphene became prevalent (Zhang et al. 2005; Novoselov et al. 2005, 2007; De Heer et al. 2007). It was evident that QHR measurements could be graphene-based, with fabrications performed by chemical vapor deposition (CVD) (Jabakhanji et al. 2014), epitaxial growth (De Heer et al. 2007; Janssen et al. 2012), and the exfoliation of graphite (Giesbers et al. 2008). Given the many methods of available graphene synthesis, efforts to find an optimal synthesis method for metrological purposes were underway. Exfoliated graphene was widely known to exhibit the highest mobilities due to its pristine crystallinity. It was a primary initial candidate as far as metrological testing was concerned. It was found in Giesbers et al. that devices constructed from flakes of graphene had low breakdown currents relative to GaAs-based counterparts, with currents on the order of 1 μA being the maximum one could apply before observing a breakdown in the QHE (Giesbers et al. 2008) (Fig. 4). AU4

Among the other forms of synthesis, epitaxial graphene (EG) proved to be the most promising for metrological applications (Tzalenchuk et al. 2010). In their work, Tzalenchuk et al. fabricated EG devices and performed precision measurements, achieving quantization uncertainties of about 3 nΩ/Ω. An example of their measurements is shown in Fig. 5, where (a) is a demonstration of how viable the graphene-based device was to be a suitable QHR standard. It was the start of a new chapter for standards, but additional work was required to exceed the stringent temperature requirement of 300 mK and low current capability of 12 μA, relative to modern day capabilities (Tzalenchuk et al. 2010). EG graphene as QHR standards soon provided increased current capability and showed impressive plateau width for high and low magnetic field and higher temperatures. EG was also synthesized on SiC via CVD in 2015, showing that graphene could provide standards-quality resistance at temperatures up to 10 K (Lafont et al. 2015). This CVD method relied on the SiC substrate to provide a template for the growth of EG from a gas containing a hydrocarbon precursor.

Establishing Graphene as a Global Resistance Standard

EG has been used as part of the traceability chain of electrical resistance dissemination in the United States since early 2017 (Janssen et al. 2011; Oe et al. 2019; Woszczyna et al. 2012; Satrapinski et al. 2013; Rigosi et al. 2019a). The preceding

Uncorrected Proof

TRIAL MODE - Click here for more information

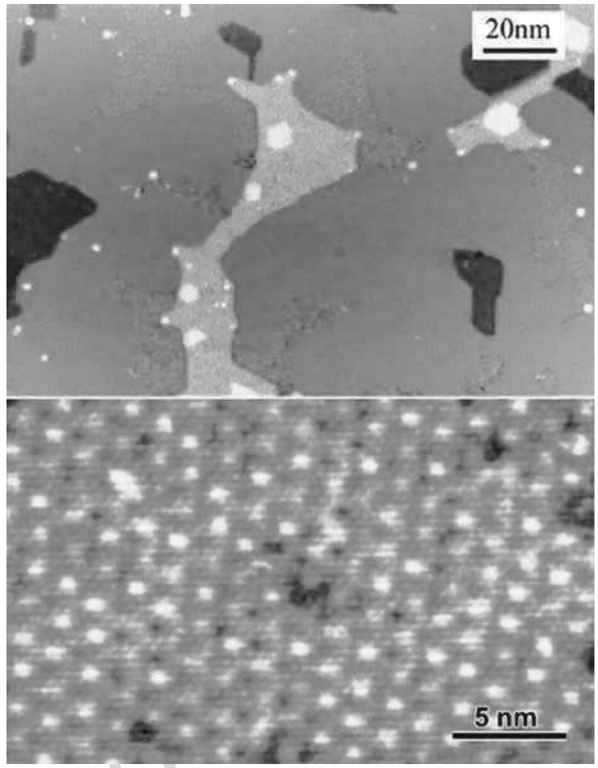

Fig. 4 Scanning tunneling microscopy images (taken at 0.8 V sample bias, 100 pA) show a single layer of epitaxially grown graphene on SiC(0001). The top and bottom panels show two different magnifications of a neighborhood of the grown crystal. (Reprinted from (De Heer et al. 2007))

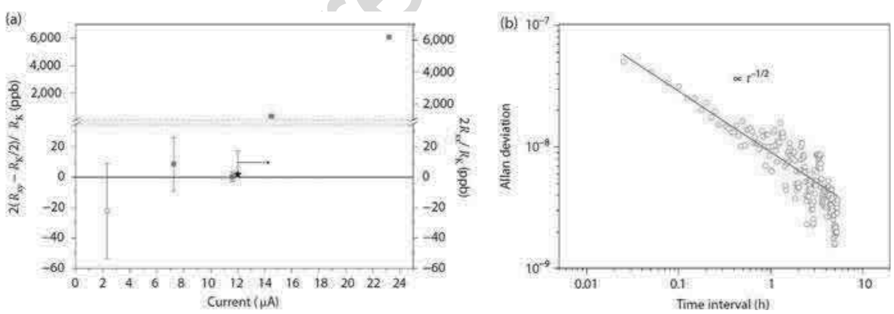

Fig. 5 The Hall resistance quantization accuracy was determined in these measurements. (**a**) The mean relative deviation of R_{xy} from $R_K/2$ is shown at different currents (ppb, or nΩ/Ω) on the right vertical axis. Recall that R_{xy} is nominally measuring the $\nu = 2$ plateau of the QHE. The value of the deviation at the smallest current was measured at 4.2 K (blue squares), and all other measurements were performed at 300 mK (red squares). To achieve the highest accuracies, using an 11.6 μA source–drain current (14 T, 300 mK), at least one of the measurements was performed over 11 h. The right vertical axis shows R_{xx}/R_K, which is represented as the black star along with its measurement uncertainty. (**b**) The Allan deviation of R_{xy} from $R_K/2$ is plotted as a function of time (of the measurement). The square root dependence (as fit by the solid red curve) is indicative of white noise. (Reprinted by permission from Springer Nature Customer Service Centre GmbH: (Tzalenchuk et al. 2010))

TRIAL MODE - Click here for more information

years from 2010 onward were dedicated to the study of basic fabrication processes and measurement techniques so that EG-based QHR devices could be accepted as the replacement for GaAs-based QHR devices. With optimized EG devices, performance far surpassed that of the best GaAs-based devices. A compilation of these efforts can be linked to multiple institutes (Lara-Avila et al. 2011; Rigosi et al. 2017, 2018, 2019b; Riedl et al. 2010; Janssen et al. 2015; Kruskopf et al. 2016; He et al. 2018). EG-based devices suitable for metrology required high-quality EG to the point of substantial scalability (centimeter-scale) as well as stabilization of electrical properties to have a long shelf life and end-user ease-of-use.

In one example of EG-based QHR development, implemented by two separate groups, devices had become compatible with a 5 T table-top cryocooler system (Rigosi et al. 2019a; Janssen et al. 2015). Janssen et al. first demonstrated this type of measurement with a table-top system in 2015, pushing the bounds of operability to lower fields and higher temperatures. The advantage of such a system also includes the removal of the need for liquid helium, enabling continuous, year-round operation of the QHR without the use of liquid cryogens. The $\nu = 2$ plateau in EG devices is the primary level used to disseminate the ohm, much like for GaAs-based QHRs. In fact, EG provides this plateau in a very robust way and for a large range of magnetic fields because of Fermi level pinning from the covalently bonded, insulating carbon layer directly beneath the conducting graphene layer (Lara-Avila et al. 2011).

For the 5 T table-top system at the National Institute of Standards and Technology (NIST), the EG QHR device plateau value was scaled to a 1 kΩ standard using a binary CCC and a DCC (Rigosi et al. 2019a). The uncertainties that were achieved with this equipment matched those obtained in GaAs-based QHR systems (i.e., on the unit order of nΩ/Ω). The results of some of these measurements are shown in Fig. 6 at three different currents. The limit of nearly 100 μA gives EG-based QHRs the edge over GaAs, especially since these measurements were performed at approximately 3 K. Another example of graphene being established as the new QHR standard comes from Lafont et al., whose work hardened the global question of when graphene would surpass GaAs in various respects (Lafont et al. 2015). An example of this investigation is shown in Fig. 7, where the sample of choice was CVD-grown epitaxial graphene on SiC. Overall, with the success of the national institute's QHR efforts, the evidence for EG-based devices surpassing GaAs-based QHRs has been widely accepted.

Uncorrected Proof

Improvements in Measurement Infrastructure

Given the establishment of better QHR devices for resistance standards, the corresponding equipment and infrastructure with which one can disseminate the ohm had to also improve or at least be shown to maintain its compatibility with EG-based QHRs. The measurement of the ratio between a QHR device and a standard resistor must achieve uncertainties that are comparable to or better than the stability of those resistors. This criterion would support the notion of reliable traceability in that system. Measurements with a longer integration time produce

TRIAL MODE - Click here for more information

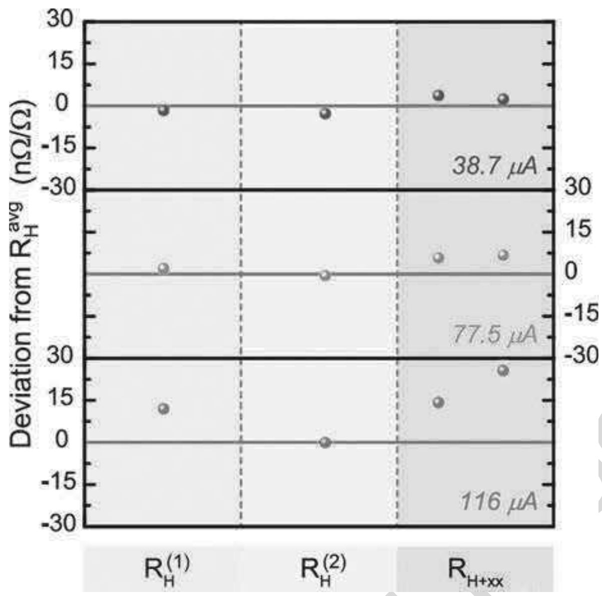

Fig. 6 Binary winding CCC measurements were performed with an EG-based QHR device in a cryogen-free table-top system at 5 T and 3 K. The CCC measurement data are displayed in three rows, with the upper, middle, and lower data corresponding to the source-drain currents of 38.7 μA, 77.5 μA, and 116 μA, respectively. Each column shows a comparison between the resistance of the $\nu = 2$ plateau and a 1 kΩ resistor, with the left two columns representing orthogonal contact pairs ($R_H^{(1)}$ and $R_H^{(2)}$). The third column represents the two diagonal pairs formed by the same contacts as the two orthogonal pairs. It is labelled as R_{H+xx} and indicates the impact of the residual longitudinal resistance. The type A measurement uncertainties are smaller than the data points, and the type B uncertainties are under 2 nΩ/Ω. (© 2019 IEEE. Reprinted, with permission, from (Rigosi et al. 2019a))

better results because the ratios are well-maintained. The obvious benefits from room-temperature bridge systems like the DCC include an ability to deliver measurements to laboratories in both NMI and non-NMI settings with greater frequently (year-round) due to their operation not requiring cryogens (MacMartin and Kusters 1996). Additionally, both DCCs and CCCs have been improved so that they are more user-friendly and automated, removing, at least in the case of the DCC, most of the dependence on specialized knowledge that one normally expects for the more complex cryogenic counterparts (Williams 2011; Drung et al. 2009). Some NMIs have shown that the automated binary-ratio CCCs have type B uncertainties below 0.001 μΩ/Ω, a useful feature when dealing with precise QHR comparisons (Sullivan and Dziuba 1974; Grohmann et al. 1974; Williams et al. 2010). CCC scaling methods can achieve resistance ratios of 4000 or more, enabling measurements for sub-nanoampere current levels, whereas DCCs achieve similar current sensitivity only with larger currents.

The DCC is a room-temperature current comparator, and this simplifies the operation and cost compared to SQUID-based CCC systems. The work by

Uncorrected Proof

TRIAL MODE - Click here for more information

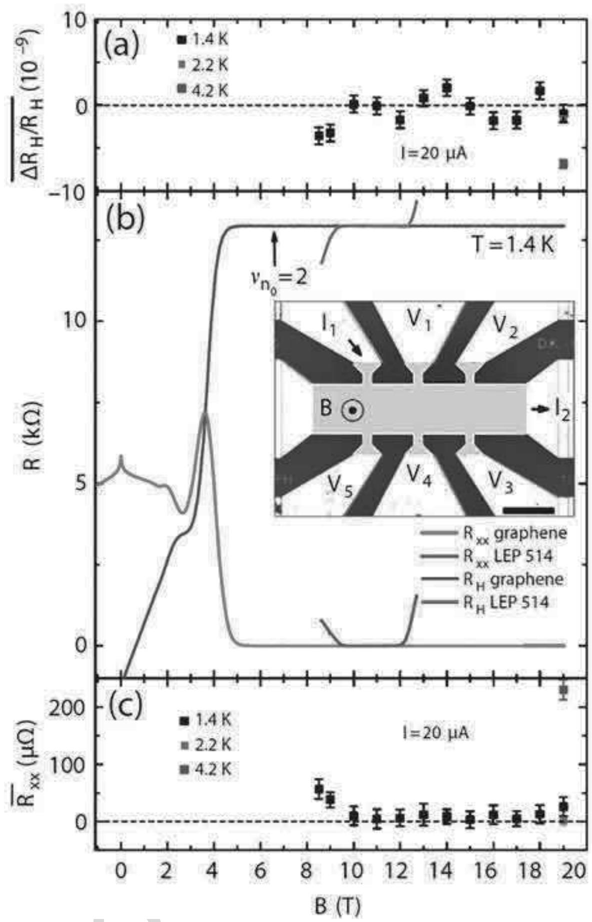

Fig. 7 The magnetic field dependence for Hall resistance in CVD-grown epitaxial graphene is shown. (**a**) The Hall resistance (R_H) deviation is measured on the $\nu = 2$ plateau at 1.4 K (black), 2.2 K (magenta), and 4.2 K (violet). (**b**) R_{xx} and R_H were measured with a source-drain current of 20 μA, with both types of voltages measured using the (V_1, V_2) and (V_2, V_3) contact pads, respectively. The magnetic field was energized to values between 1 T and 19 T for the graphene device (shown by the red and blue curves) and from 8 T to 13 T for the GaAs device (maroon and gray curves). The onset of the Landau level was calculated by using the carrier density at low magnetic fields, which is related to the slope of R_H near zero field. The inset shows an optical image of the device (scale bar is 100 mm). (**c**) Data for precision measurements of R_{xx} are shown at 1.4 K (black), 2.2 K (magenta), and 4.2 K (violet). The error bars represent combined standard uncertainties (1σ). (Lafont et al. (2015) is an open-access article distributed under the terms of the Creative Commons CC BY license, which permits unrestricted use, distribution, and reproduction in any medium)

MacMartin and Kusters shows the development of a DCC for comparing four-terminal resistances (MacMartin and Kusters 1996). It works by measuring a current ratio, represented as a turns ratio, that is balanced by detecting magnetic hysteresis in magnetic cores using a modulator. Manual dials allowed the ratio to be adjustable in

TRIAL MODE - Click here for more information

part-per-million steps. The two current sources in the DCC are isolated so that there is no current in the galvanometer circuit when fully balanced. Their DCC was able to measure and compare the ratio of two isolated direct currents and adjust the ratio to balance the galvanometer. A detailed description provided a discussion of its accuracy limitations (MacMartin and Kusters 1996). In the optimum operating range, the authors achieved accuracies that were better than one part per million. The bridge was designed to accommodate the scaling of resistance standards from 100 Ω to a less than 1 mΩ and can be used for any ratio from 1 to 1000, thus permitting one to calibrate low value resistors and current shunts whose accuracies would be limited only by the level of noise and the stability of the resistor (MacMartin and Kusters 1996). Modern DCC systems are fully automated to control current levels, ratios, and resistance values, and allow scaling of resistance standards from 100 kΩ to below 10 μΩ.

From the previously mentioned work at NIST (Rigosi et al. 2019a), the two bridges demonstrate the applicability of using a modern room-temperature DCC with an EG-based QHR device to obtain uncertainty near 0.01 mΩ/Ω. As shown in Fig. 8a, the DCC measurements extend the range of the applied source-drain currents when scaled from the EG-based QHR device to a 1 kΩ resistor. The inset of Fig. 8a shows how sample heating from a high applied current affects the overall sample temperature. This information was relevant because high currents applied to EG-based QHR devices improves the resolution of the DCC measurements, but will degrade the accuracy of the QHE due to too high a temperature. Ultimately, the work found that table-top systems, in which the QHR is cooled indirectly by conduction and is in vacuum, may limit how much current can be applied (Rigosi et al. 2019a). Larger cryomechanical chillers are designed to immerse the device in a small volume of liquid helium and provide better temperature stabilization by contact with the liquid bath.

As of the present day, CCC bridges outperform DCCs in terms of achievable uncertainties. However, in order to more easily disseminate QHR technology globally, room temperature DCCs are preferred in terms of ease-of-use and fewer resource needs as well as year-round operability. For this reason, a comparison between the two methods was examined and is shown in Fig. 8b, where the number of DCC data points averaged was varied inversely with the square of the applied voltage $V \approx I_{SD} \times R_H$ to obtain a similar type A uncertainty for all values of the source-drain current, with measurement durations ranging from 110 min for the 0.5 V measurements to 24 min for the 1.2 V measurements. Further, in Fig. 8b, the uncertainties indicated in blue were produced by the DCC software. The larger, red error bars are uncertainties that take into account known statistical correlations in the data (Zhang 2006). Potential noise from the cryogen-free mechanical refrigeration system may also interfere to some degree with the balancing algorithm. A similar issue exists for CCC systems, where the additional noise from vibration may increase noise and may cause the SQUID to lose the delicate balance required to maintain its set point through feedback.

Even though DCCs would make global dissemination easier for some research institutes and smaller NMIs, CCC technology is still important for international metrology at the highest levels. Williams et al. demonstrated a design for an

Uncorrected Proof

TRIAL MODE - Click here for more information

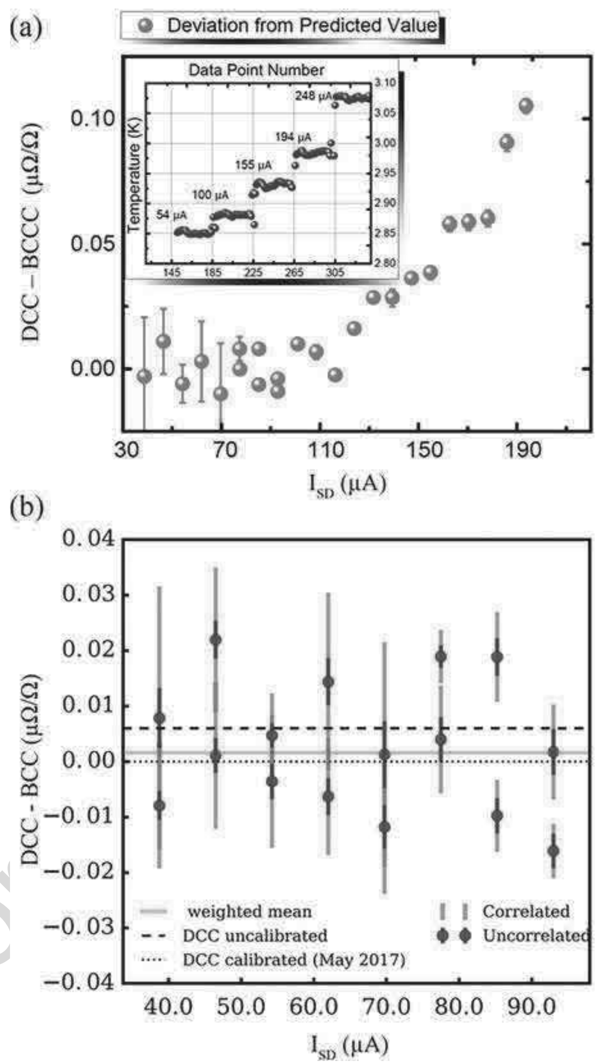

Fig. 8 (**a**) Current dependence data of DCC ratios for a 1 kΩ resistor are shown in magenta, based on the same EG QHR device used with a binary winding CCC (BCC). The DCC results confirm that the QHR device remains quantized to within 0.01 μΩ/Ω up to approximately 116 μA. Data for higher source-drain currents shows the effect of heating of the sample caused by power dissipation, with temperature data for extended current ranges shown in the inset with blue data points. Some type A measurement uncertainties (in red) are smaller than the data points. (**b**) DCC data for the ratio of the QHR to 1 kΩ are shown for increasing source-drain currents from 38 μA to 94 μA and are normalized to the average results of BCC scaling (using 38.7 μA and 77.5 μA). The red error bars show the expanded ($k = 2$) with uncorrelated uncertainties whereas the blue error bars show the expanded ($k = 2$) uncertainty reported by the measurement device. (© 2019 IEEE. Reprinted, with permission, from (Rigosi et al. 2019a))

Unco

automated CCC in order to perform routine NMI measurements (Williams et al. 2010). Their system uses a CCC in a low loss liquid helium storage vessel and may be continuously operated with isolated supplies coming from the mains power. All parameters were shown to be digitally controlled, and the noise sources present in the system were analyzed using the standard Allan deviation, leading to the conclusion that one may eliminate non-white noise sources simply by choosing the appropriate current reversal rate. New generations of CCC systems with integrated fast ramping current sources, nano-voltmeter, and a compensation network for improved bridge balancing have become widely used at worldwide NMIs (Drung et al. 2009).

TRIAL MODE - Click here for more information

As progress continues, NMIs have both anticipated and in many cases achieved these goals for EG-based QHR devices. Lastly, to begin expanding on the functionality of EG-based devices, it would need to be shown that precise resistance scaling could be done to reference resistors from the QHR by using voltages larger than those available in standard DCCs and CCCs. These efforts are underway and hope to eventually accelerate dissemination efforts.

Expanding the Use of the Quantum Hall Effect in Graphene

Assembly of p-n Junctions in Graphene-Based Devices

With EG-based QHR devices established as national standards at several NMIs, as well as the metrology community in agreement that comparisons against GaAs-based QHR devices had been accomplished, the next steps became clearer concerning how the EG-based QHR could be further developed. Unlike the QHR in GaAs, only the $\nu = 2$ plateau is well quantized, and although other Landau levels exist in graphene, they simply do not offer the same level of precision as the $\nu = 2$ plateau (Zhang et al. 2005; Hu et al. 2021). Since the early 1990s, it has been of interest that QHR devices have a means of interconnecting several single Hall bar elements without loss of precision, and this has since been of great research interest. As discussed earlier, this work allowed QHR devices to output more than the single value at the $\nu = 2$ plateau (about 12.9 kΩ) through arrays of devices, using what are described as multi-series interconnections (Delahaye 1993). With graphene, which supports both electron conduction and hole conduction (with positive carrier charge) the first natural question is whether one may use the plateau at $\nu = -2$, in addition to the plateau at $\nu = 2$. This array would avoid the need for manufactured interconnections entirely, using an interface of electronic states internal to the 2D conductor.

This alternative for outputting new quantized values utilizes *p-n* junctions (*pn*Js) to provide useful and controllable values of resistance quantization (Hu et al. 2018a, b; Woszczyna et al. 2011; Rigosi et al. 2019c; Momtaz et al. 2020). Woszczyna et al. approached this issue a decade ago (Woszczyna et al. 2011), noting that since metallic leads had to cross paths in traditional GaAs-based devices, typical fabrication methods would be overly complicated, having to include some form of multilayer interconnect technology. Any leakage between leads would likely generate an additional Hall voltage, thus becoming a detriment to the achievable uncertainty. Graphene is more accessible for the fabrication of small structures than the GaAs heterostructure interface, where contacts must be alloyed through the insulating surface layer. Charge carrier control by gating offered the opportunity to combine two regions of opposite charge carrier polarity. Rather than requiring interconnections, such a device only needs a set of uniform top gates to modulate regions between the $\nu = -2$ and $\nu = 2$ plateaus. This work demonstrated that *pn*Js were possible and worth exploring as a viable extension for QHR standards.

The fabrication of *pn*J devices larger than the order 100 μm is presently limited by the difficulty of producing of high-quality, exfoliated single-crystal hexagonal boron nitrate (*h*-BN) as an insulating material for top gating. As demonstrated by Hu et al.,

Uncorrected Proof

TRIAL MODE - Click here for more information

numerous pnJ's can be fabricated in a single device of size 100 μm or less, rendering it possible to implement reliable top gates for adjusting the carrier density in gated EG-based devices (Hu et al. 2018a). The underlying physics of these *pn*Js makes it possible to construct devices that can access quantized resistance values that are fractional or integer multiples of R_K. Hu et al. made an assessment for one such *pn*J device at the $\nu = -2$ and $\nu = 2$ plateaus (summing to about 25.8 kΩ), with data shown in Fig. 9. A DCC was used to provide turn-key resistance traceability and compare against a 10 kΩ standard resistor (see Fig. 9a). The measurement time for each data point with the DCC was 15 min, with an orange shaded region representing Fig. 9b, which clarifies the deviation of the DCC measurements with respect to zero. In Fig. 9a, the right axis is represented by black points and gives the relative uncertainty of each measurement as a function of source-drain current. For this *pn*J device, a precision of about 2×10^7 was achieved as shown in Fig. 9b. Although this may be one or two orders of magnitude below what is possible for a conventional Hall bar device, one must recall that, based on this work, a programmable resistance standard may be built using the demonstrated techniques. Such flexibility and expansion of accessible parameter space could justify its further technical exploration within resistance metrology.

These types of devices are not as well-studied as other conventionally prepared devices, but given their interesting and rather unique properties, *pn*J devices could

Uncorrected Proof

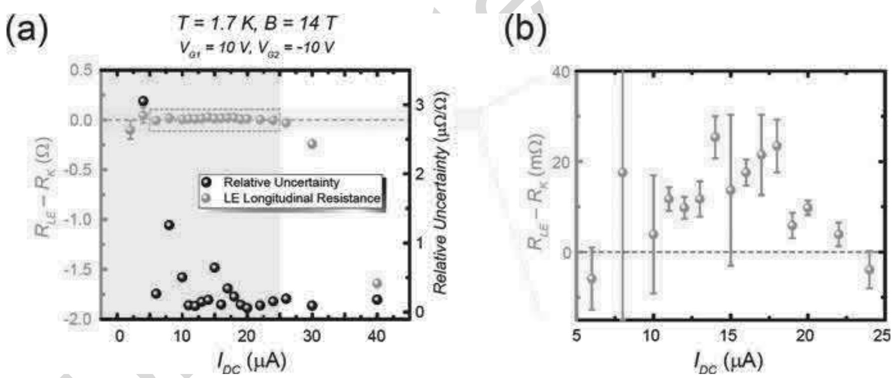

Fig. 9 (**a**) The lower edge (LE) of the device in Hu et al. was compared against a 10 kΩ standard resistor with a DCC to give an assessment of the quality of quantization exhibited by the device. The resistor was selected based on its traceability to a quantum resistance standard at the National Institute of Standards and Technology. The turquoise points show the DCC measurements as deviations from R_K on the left axis and the relative uncertainties of those deviations with DC current. The relative uncertainties improve with increasing current, but the device loses its optimal quantization after the critical current of 24 μA. The shaded green area indicates the well-quantized region. (**b**) The beige shaded area in (**a**) is magnified to show the deviations' error bars as well as the reference to zero deviation, marked as an orange dashed line. The error bars represent a 1σ deviation from the mean, where each data point represents an average of a set of data taken at each value of current. (Hu et al. (2018a) is an open access article distributed under the terms of the Creative Commons CC BY license, which permits unrestricted use, distribution, and reproduction in any medium)

TRIAL MODE - Click here for more information

offer a second, more fundamental path to avoid any resistance from interconnecting metallic contacts and multiple device connections. This possibility is illustrated in a recent experiment by Momtaz et al. and demonstrates how a programmable quantum Hall circuit could implement an iterative voltage bisection scheme, thus permitting the user to access any binary fraction of the $\nu = 2$ plateau resistance (Momtaz et al. 2020). Their proposed circuit designs offer potential advantages for resistance metrology, as summarized here: first, their circuit contains no internal Ohmic contacts, a recurring problem in interconnected QHR circuits. Second, there is a logarithmic scaling of the complexity of the design as a function of the required fractional resolution. This scaling feature is a major advantage compared with a standard QHARS device. The latter might use hundreds of distinct multi-contact Hall bars, whereas a bisection circuit can output a similar number of values while only needing a small number of elements. The approach is thought to match, or become comparable to, the present limits of QHR standards.

The design does have some limitations, as pointed out by Momtaz et al. They noted that, even though the last bisection stages of the device were controlling a finer portion of the output value, each stage still relied on QHE states equilibrating across a junction barrier, emphasizing the importance of the quality of the junction itself. Their preliminary numerical estimates suggest that imperfections in the device would be partially fixable since any absolute errors caused by imperfect mixing would not be amplified through the remaining sections of the device. Nonetheless, this design warrants further study as one way to expand on available quantized resistance outputs.

Using Arrays to Expand the Parameter Space

Recent developments have utilized superconducting materials like NbN and NbTiN to create interconnections compatible with EG-based QHR devices (Kruskopf et al. 2019a, b; He et al. 2021). These metals have high critical temperature (≈10 K) and critical field (≈20 T) so that they may be applied to QHR devices during measurement, as shown by Kruskopf et al. (2019b). They argue that array technology based on superconducting metals is preferred and can eliminate accumulated resistance and voltage errors at contacts and interconnections. They demonstrated that the application of NbTiN, along with superconducting split contacts, enabled both four-terminal and two-terminal precision measurements without the need for insulated crossovers. The split contacts are inspired by the multiple series approach described by Delahaye (1993), with reduced separation between the interconnections. Since the resulting contact resistances become much smaller than R_{K}, it becomes straightforward to fabricate series and parallel connections as fundamental device elements. The limits of this technology have not yet been determined, nonetheless, the merits of this technique seem to point to such structures as the next generation of QHR devices.

Another example of array technology that expands on the parameter space comes from Park et al. (2020), where they successfully construct 10 single Hall bars in series with EG on SiC. They operated this device at the $\nu = 2$ plateau near 129 kΩ

Uncorrected Proof

TRIAL MODE - Click here for more information

with precision measurements made using a CCC. While measuring the device at a magnetic field of 6 T and a temperature of 4 K, they were able to achieve a relative uncertainty of approximately 4×10^{-8}, approaching the state-of-the-art for this resistance level. Despite only being able to inject a low double-digit electrical current (in μA), their efforts added support to the notion of expanding QHR values with QHARS devices.

One difficulty that could arise from making these arrays, especially as they increase in lateral size, is how to make their carrier densities uniform. For that, there are two prime examples of accomplishing this task, with both methods being user-friendly and attaining a long shelf life for the device. The first method involves functionalizing the EG surface with $Cr(CO)_3$ (Rigosi et al. 2019b), and what this process enables the user to do is apply heat for a specified time to obtain a predictable carrier density. The advantage is that this process is reversible and may be cycled without damaging the device. One of the features of this method is that storing the device in air for long periods of time simply resets the Fermi level to an energy close to the Dirac point. The same anneal may be applied to reacquire the value of the carrier density. Once in an inert environment or at colder temperatures, the carrier density of the device remains stable. The second method involves a polymer-assisted doping process (He et al. 2018), which allows the user to adjust the carrier density by also using an anneal. This method retains some reversibility as long as the polymer will retain its matrix. Both methods are highly scalable and give extended shelf life to EG-based standards.

With the ability to make very large QHARS devices having controllable and uniform carrier densities, researchers were able to construct a 1 kΩ array based on 13 single Hall bar elements in parallel (Hu et al. 2021). A CCC was used to measure two 13-element arrays. At 1.6 K, the array devices achieved useful quantization above 5 T. One such array measurement is shown in Fig. 10. In this case, the DCC measurements verified that, in the high-field limit, the resistance for both *B*-field directions approached the value $R_K/26$ (about 992.8 Ω) to better than one part in 10^8 for currents up to 700 μA. As is typical, the CCC ratio uncertainty was below one part in 10^9, and most of the uncertainty had originated from the 100 Ω artifact resistance standards (Fig. 11).

Recent work by He et al. shows quantum Hall measurements performed on a large QHARS device containing 236 individual EG Hall bars (He et al. 2021). Given the difficulty of verifying the longitudinal resistance as zero for every element, they utilized a direct comparison between two similar EG-based QHARS devices to verify the accuracy of quantization. The design of this array is such that two subarrays with 118 parallel elements are connected in series, having a nominal resistance of $h/236e^2$ (about 109.4 Ω) at the $\nu = 2$ plateau. The Hall bars were designed to be circular in order to both have a symmetrical design and to be able to fit many devices into a small area (He et al. 2021). The contact pads and interconnections were fabricated from NbN and support currents on the order of 10 mA at 2 K and 5 T. Additionally, a split contact design was implemented to minimize the contact resistance, much like other previously reported work (Kruskopf et al. 2019a, b). The two QHARS devices were compared using high precision

Uncorrected Proof

TRIAL MODE - Click here for more information

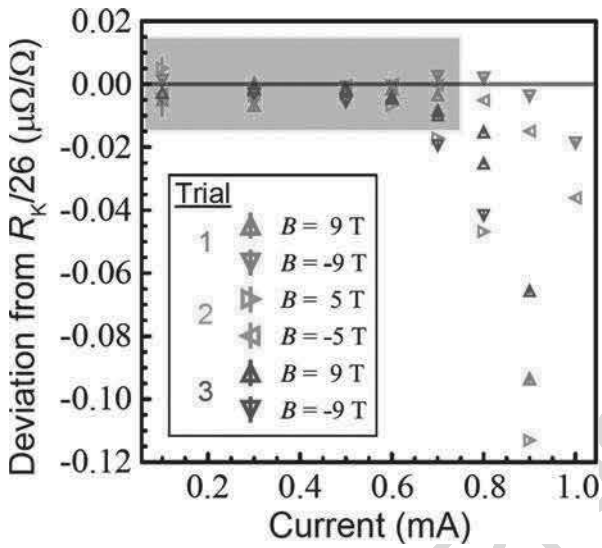

Fig. 10 The $\nu = 2$ plateau was measured at selected values of the magnetic field (B) for device 1 at 1.6 K in a conventional cryostat using a room-temperature DCC. DCC measurements verify that, in the high-field limit, the resistance for both B-field directions approaches the value $R_K/26$ (about 992.8 Ω) to better than one part in 10^8 for currents up to 700 μA, confirming that this array device utilizes highly homogeneous graphene. All expanded uncertainty values given here are for a 2σ confidence interval. (Hu et al. (2021) is an open access article distributed under the terms of the Creative Commons CC BY license, which permits unrestricted use, distribution, and reproduction in any medium)

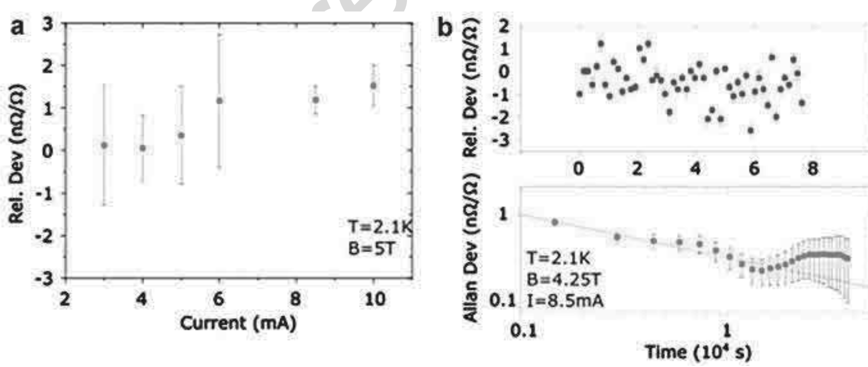

Fig. 11 High bias current measurements on arrays. (**a**) CCC measurements are shown of a direct comparison between subarrays to show that no significant deviation occurs until 8.5 mA. The data consist of the mean of 5–10 CCC readings, each of which is 20 min long. The top graph shows the relative deviation, with error bars of one standard deviation. The bottom graph shows the corresponding Allan deviation. The standard error is limited to 0.25 nΩ/Ω. (He et al. (2021) is an open access article distributed under the terms of the Creative Commons CC BY license, which permits unrestricted use, distribution, and reproduction in any medium)

Corrected Proof

TRIAL MODE - Click here for more information

measurements, showing no significant deviation of their output resistance within 0.2 nΩ/Ω. Within the next few years, given the increasing complexity of EG-based QHARS devices, even larger and more versatile arrays are expected to make available an abundance of new quantized resistance values.

From DC to AC to the Quantum Ampere

As the *quantum* SI continues to expand in its applications, new research directions are plentiful and of interest to the electrical metrology community. The QHE will continue to be our foundation for disseminating the ohm in the DC realm. The vast improvements in EG-based QHR technology are beginning to inspire efforts to develop more sophisticated devices suitable for AC resistance standards. This subfield of electrical metrology focuses on the calibration of impedance and is conventionally obtained from systems like a calculable capacitor (Thompson and Lampard 1956; Clothier 1965; Cutkosky 1974). Such a system has allowed for the calibration of capacitors, inductors, or AC resistors, which is essentially a measurement of complex ratios of impedance, where the signal phase depends on the type of standard. Historically, the design and operation of this kind of system have been challenging because of unavoidable fringe electric fields, imperfections in capacitor electrode construction, and a long chain of required bridges and standards.

The next step for improving AC standards may be to introduce EG-based QHR devices, as Kruskopf et al. have done recently (Kruskopf et al. 2021). They used a conventional EG-based device to analyze the frequency dependence of losses and to determine the characteristic internal capacitances. The environment of the device included a double shield used as an active electrode, to compensate for capacitive effects, as shown in Fig. 12a. Figure 12b displays the set of magnetocapacitance measurements corresponding to a configuration of the capacitance (*Cx*) between the active electrode (left side of (a)) and the EG Hall bar between points A and B in Fig. 12a. *Cx* was compared with a variable precision reference capacitor using a simple configuration used for other traditional measurements (Kruskopf et al. 2021). Figure 12a shows the passive electrode on right side, shorted to the EG contact, and therefore not contributing to the measurement of *Cx*.

The AC QHR may directly access the units of capacitance and inductance with high precision (Kruskopf et al. 2021; Lüönd et al. 2017). Kruskopf et al. show the voltage and frequency dependencies of the magnetocapacitance in Fig. 12b, c, respectively, along with the associated dissipation factor for an example device. By appropriately modeling the compressible and incompressible states, the observed dissipation factors may be explained rather well. At low magnetic field values, the 2D electron system in the EG is not quantized and is thus accurately representable as a semi-metal with dominant compressible states. However, when the magnetic field is increased, *Cx* starts to decrease around 4 T and does so by nearly 3 fF in both cases as 12 T is approached. This phenomenon may be due to the increase in incompressible regions that form, which are themselves transparent to electric fields. Furthermore, the dissipation factor is observed to first increase, peaking during the transition

Uncorrected Proof

TRIAL MODE - Click here for more information

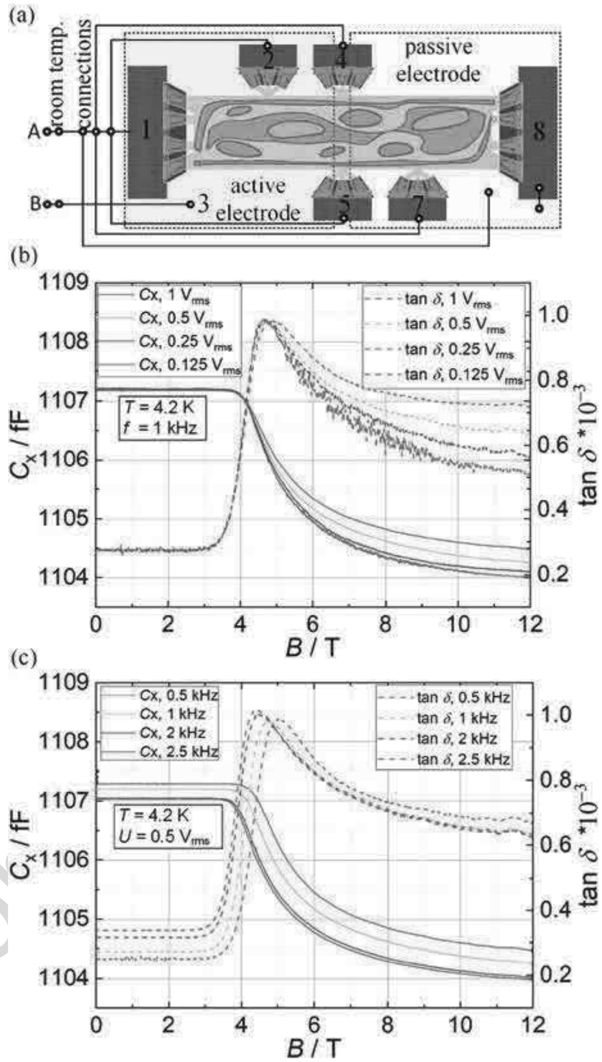

Fig. 12 Magnetocapacitance measurement data of an example device are shown (taken at 4.2 K). (**a**) An illustration captures the various elements of the used magnetocapacitance measurement configuration. As one electrode gets shorted to the labeled passive electrode (pin 8), the other electrode is then used to characterize C and tan(δ). Compressible and incompressible states of the 2D electron system are represented as different colors within the EG Hall bar. (**b**) The capacitance is plotted as a function of magnetic field for a set of different voltages. (**c**) A similar plot to (**b**) is shown for a set of different frequencies. The dissipation factor (tan(δ)) is also plotted representing the losses between the active electrode and the EG Hall bar device. (Kruskopf et al. (2021) is an open access article distributed under the terms of the Creative Commons CC BY license, which permits unrestricted use, distribution, and reproduction in any medium)

region as the resistance plateau in EG forms. As the quantization accuracy improves at higher magnetic fields, the observed dissipative losses decrease again to about tan (δ) = 0.0003. Overall, these are but a few magnetocapacitance measurements that demonstrate the viability of efforts to better understand the physical phenomena driving the observations made in the QHE regime while under AC conditions. This pursuit of AC QHR standards aims to advance how units such as the farad and henry are realized by using fundamental constants instead of dimensional measurements.

In addition to expanding the influence of the QHE to AC electrical metrology, one may also expand into the realms of electrical current and mass metrology by utilizing

TRIAL MODE - Click here for more information

EG-based QHARS devices. The realization of the quantum ampere lacks accurate traceability to within 10^{-8} despite the various efforts that exist for developing a current source using single-electron tunneling devices (Giblin et al. 2012; Pekola et al. 2013; Koppinen et al. 2012). The alternative route one may take to realizing the quantum ampere is by building a circuit that effectively combines the QHE and a programmable Josephson junction voltage standard. This combination has been recently assembled to attain a programmable quantum current generator, which may disseminate the ampere at the milliampere range and above (Brun-Picard et al. 2016). The work reported by Brun-Picard et al. demonstrates this construction with a superconducting cryogenic amplifier and to measurement uncertainties of 10^{-8}. Their quantum current source, which is housed as two separate cryogenic systems, can deliver accurate currents down to the microampere range. Considering the orders of magnitude involved, this work renders the programmable quantum current generator a pronounced supplement to electron-pumping mechanisms.

Future Improvements and the Quantum Anomalous Hall Effect

Limitations to the Modern QHR Technology

In order to make an accurate assessment of future needs for quantum metrological applications, it would benefit us to know the limits of the current technology, at least to some extent. For instance, it is not known with substantial certainty how high a current could be applied to a single EG Hall bar, or the upper bound on operational temperature for EG-based devices.

There is much research to be conducted on newer technologies that build on the single Hall bar design despite the noted benefits from their development. For instance, the *pn*J devices have conceptual access to different fractional or integer multiples of R_{H} (or $R_{\mathrm{K}}/2$) as possible resistances, especially if source and drain currents are allowed for more than two total terminals. If one defines q as a coefficient of $\mathrm{R_H}$, then the following relation may be used (Rigosi et al. 2020):

$$q_{M-1}(n_{M-1}) = \frac{q_{M-2}(n_{M-1}+1)}{n_{M-1} + \frac{q_{M-2}}{q_{M-1}^{(0)}}} \tag{1}$$

In Eq. (1), M is the number of terminals in the *pn*J device, n is the number of junctions between the outermost terminal and its nearest neighbor, and $q_{M-1}^{(0)}$ refers to a default value the device outputs when the configuration in question is modified such that its outermost terminal moves to share the same region as its nearest neighbor (meaning that one of the two outermost regions containing any source or drain terminals has both a source and a drain connected to it) (Rigosi et al. 2020). The key takeaway with this algorithm (Eq. 1) is that an incredibly vast set of available resistances becomes hypothetically possible by simple reverse engineering.

Uncorrected Proof

TRIAL MODE - Click here for more information

The algorithm assumes that the Hall bar is of conventional linearity. That is, each *p* region is adjacent to two other *n* regions unless it is an endpoint. The same would hold true when *p* and *n* are swapped. The equation breaks down when the *pn*J device geometry changes to that of a checkerboard grid or Corbino-type geometry. In all of these cases, the available resistances in this parameter space are vastly abundant and will obviously not be a limiting factor for this species of device. Instead, limitations may stem from imperfections in the device fabrication, an almost inevitable manifestation as the device complexity increases (Rigosi et al. 2019c).

In the limit of the purely hypothetical, should the resistance metrology community wish to scale to decade values only, as per the existing infrastructure, then a programmable resistance standard may be able to provide many decades of quantized resistance output by following the designs proposed by Hu et al. (2018a). The proposed programmable QHR device is illustrated in Fig. 13, with each subfigure defining a small component of a total device. When programmed in a particular way, this single device can output all decades between 100 Ω and 100 MΩ, as summarized by Table 1 (where voltage probes are labeled in reference to Fig. 13c).

With all *pn*J devices, better gating techniques are warranted. In the case of top gating, which is the basis for forming the device measured by Hu et al. (2018a), fabrication is limited by the size of the exfoliated *h*-BN flake typically used as a high-quality dielectric spacer. For bottom gating of EG on SiC, as seen with ion implantation (Waldmann et al. 2011), there has not yet been a demonstration of metrologically viable devices, though there may still be potential for perfecting this technique. Since gating is likely to be the largest limiting factor for *pn*Js, one must instead turn to array technology. Although QHARS devices can theoretically replicate *pn*Js, the necessity of an interconnection will ultimately result in a smaller available parameter space. Nonetheless, the output quantized resistance values offered by this technology may still be sufficiently plentiful for future applications in electrical metrology.

When it comes to arrays, there are several types that can take shape for a potential QHR device. There are the conventional parallel or series devices, which are the subject of recent works (Hu et al. 2021; Kruskopf et al. 2019a, b; He et al. 2021; Park et al. 2020). As one departs from this simpler design, the number of potential quantized resistances that become available rapidly increases. Designs with varying topological genera, as shown in Fig. 14, along with the predictive power of simulations like LTspice, Kwant, or traditional tight-binding Hamiltonians, allows the designer to customize devices accordingly. Depending on the genus and final layout, QHARS devices can still be metrologically verified by means of measuring a specific configuration and its mirror symmetric counterparts. In that sense, future QHARS devices whose longitudinal resistances cannot be checked must either be compared with a duplicate of itself, or must have appropriate symmetries such that a same-device comparison can be made. For instance, a square array could be the subject of a two-terminal measurement using same-sided corners. This configuration would have a four-fold symmetry which can be measured and compared to verify

Uncorrected Proof

TRIAL MODE - Click here for more information

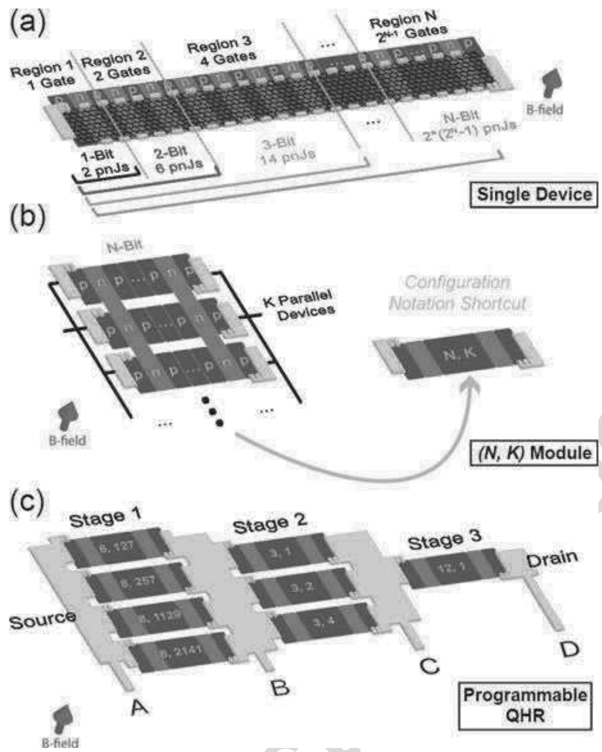

Fig. 13 The proposed device illustrated represents a programmable QHR device for scalable standards. (**a**) An *N-bit* device is illustrated showing how each region is defined and the maximum number of *pn*Js that can be used. (**b**) This device, when connected in parallel with *K* copies of itself, becomes the foundation of the (*N*, *K*) *module*. Each region has a set of gates that extend to all *K* parallel branches. (**c**) The proposed device is illustrated and composed of eight (*N*, *K*) *modules*, four of which are in parallel in stage 1, three of which are parallel in stage 2, and a single *module* in stage 3. All three stages are connected in series and all connections and contacts are proposed to be superconducting metal to eliminate the contact voltage differences to the greatest possible extent. The *modules* in stage 1 are *8-bit* devices with more than 100 parallel copies per *module*, whereas the *modules* in stage 2 are *3-bit* devices with four or fewer parallel copies per *module*. Stage 3 is a single *12-bit* device with no additional parallel branches. These numbers for (*N*, *K*) are required should one wish to reproduce the values in Table 1. (Hu et al. (2018a) is an open access article distributed under the terms of the Creative Commons CC BY license, which permits unrestricted use, distribution, and reproduction in any medium)

device functionality. All types of arrays would be thus limited by the EG growth area, which at present has been optimized by the use of a polymer-assisted sublimation growth technique (Kruskopf et al. 2016). The total growth area may be the most demanding limiting factor for this species of device. Nonetheless, one can hope that the latter technique, and any similar technique to be developed, will enable homogeneous growth on the wafer scale such that the whole EG area retains metrological quality.

Uncorrected Proof

TRIAL MODE - Click here for more information

Table 1 This shows all possible resistance decades achievable with the proposed programmable QHR device in Fig. 13

Resistance	Stage 1	Stage 2	Stage 3	Voltage probes used	Deviation from decade value
100 Ω	00010010 00011001 00001001 00010001	None	None	*A, B*	0.714 μΩ/Ω
1 kΩ	10001001 10001011 10000111 10010001	None	None	*A, B*	0.108 μΩ/Ω
10 kΩ	00110001 00100111 00110011 00111100	011 010 010	None	*A, C*	14.8 nΩ/Ω
100 kΩ	00111101 00111101 00111100 00111110	010 010 010	000000000011	*A, D*	0.043 nΩ/Ω
1 MΩ	00101011 00100001 00110101 00110000	010 001 001	000000100110	*A, D*	0.0243 nΩ/Ω
10 MΩ	01011110 01011001 01010011 01001100	110 101 110	000110000010	*A, D*	0.346 pΩ/Ω
100 MΩ	01110111 10001001 01101101 01100111	100 011 011	111100100001	*A, D*	1.21 nΩ/Ω

The values listed in this table are described in more detail in Hu et al. (2018a) and can achieve values of seven decades of resistance. Each module in each stage is assigned a binary string. As long as the exact configuration is used, the measured voltage between the two probes will measure a near-exact decade value, to within a deviation defined in the rightmost column. Hu et al. (2018a) is an open access article distributed under the terms of the Creative Commons CC BY license, which permits unrestricted use, distribution, and reproduction in any medium

Uncorrected Proof

The Quantum Anomalous Hall Effect

Regardless of EG device size, the magnetic field requirement will always be a limit. This is inherently tied to the band structure of graphene. In addition to this limitation, there are at least two others that prevent SI-traceable quantum electrical standards beyond the ohm from being user-friendly and more widely disseminated, which at present, confines their global accessibility to mostly NMIs. These other limitations include the sub-nA currents obtained from single electron transistors (in the case of the quantum ampere) and the Josephson voltage standard's aversion to magnetism, complicating the use in a single cryostat with a QHR device to create a compact

TRIAL MODE - Click here for more information

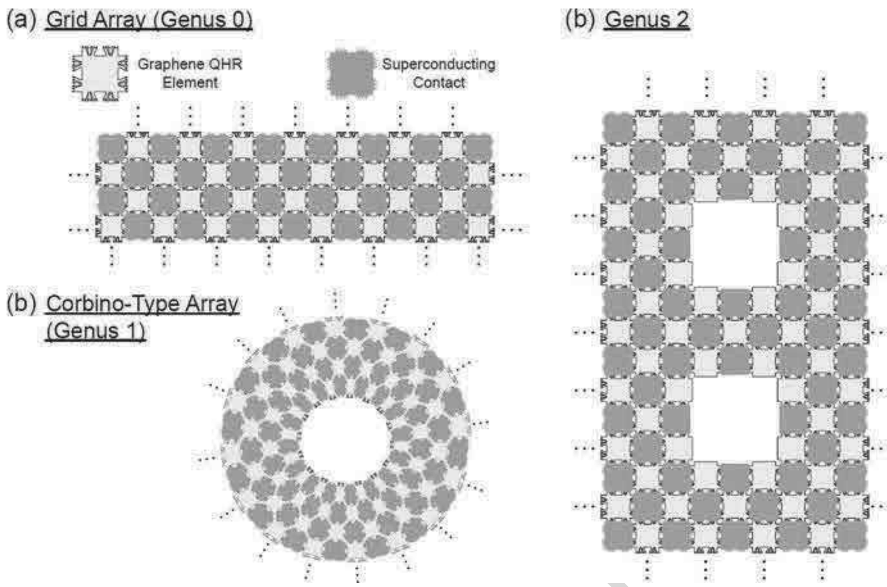

Fig. 14 Hypothetical array designs of varying topological genera. Determining the predicted value of output quantized resistance between any pair of contacts can be done with various modeling techniques done for similar systems. (**a**) The use of superconducting contacts enables the design of larger and more complex arrays, provided the EG QHR elements are small enough. For genus 0, grid arrays can take on user-defined dimensions. (**b**) Corbino-type geometries could also be implemented, and these are just examples of genus 1 topologies. (**c**) A final example of array type comes from those that have a genus 2 topology. Even more customized designs are possible and not well-explored

current standard. Ongoing research on magnetic topological materials has the potential to avoid compatibility problems.

The physical phenomenon underpinning this research is the quantum anomalous Hall effect (QAHE). This effect yields a quantized conductance in magnetically ordered materials at zero applied magnetic field. Certain types of material display a quantized resistance plateau at zero-field suitable for metrology measurements, as has been shown in some recent work (Fox et al. 2018; Götz et al. 2018). The QAHE is a manifestation of a material's topologically nontrivial electronic structure. The QAHE, along with the Josephson effect and QHE, is a rare example of a macroscopic quantum phenomenon. There are several types of materials that exhibit the QAHE, with many being classified within the following categories: magnetically doped topological insulators (TIs), intrinsic magnetic TIs, and twisted van der Waals layered systems.

Fox et al. explored the potential of the QAHE in a magnetic TI thin film for metrological applications. Using a CCC system, they measured the quantization of the Hall resistance to within one part per million and, at lower current bias, measured the longitudinal resistivity under 10 mΩ at zero magnetic field (Fox et al. 2018). An example of the data they acquired is in Fig. 15a, b. When the current density was

TRIAL MODE - Click here for more information

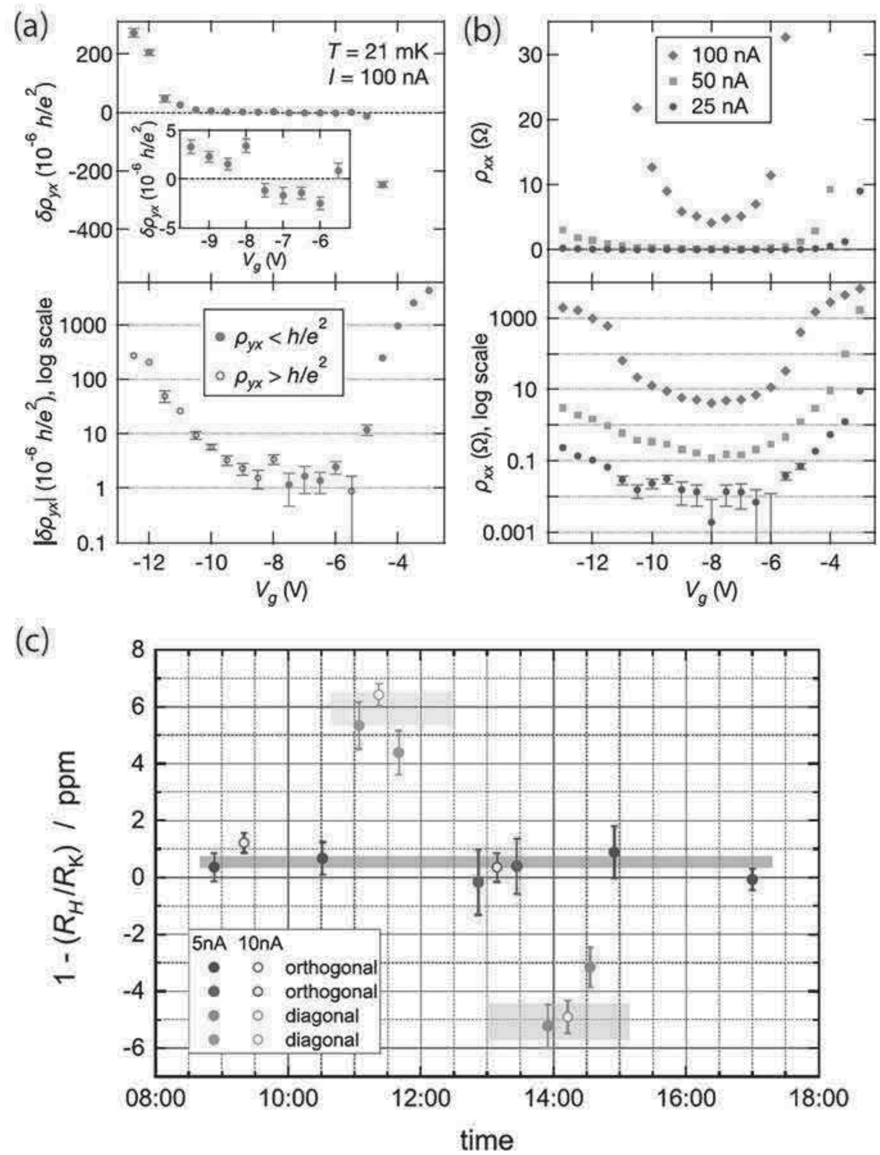

Fig. 15 (**a**) CCC data are shown for measurements of ρ_{yx} in an example device using a 100 nA current at 21 mK. The plateau in the upper panel shows the deviation from R_K for a range of gate voltages. The inset shows a magnified view of the Hall resistance deviations in the center of the plateau ($\nu = 1$). The bottom panel shows the logarithmic behavior of the deviations as one departs from the optimal gate voltage. (**b**) ρ_{xx} of the same device was measured as a function of gate voltage for three different bias currents. The data show strong current and gate voltage dependence, as displayed on a linear and log scale in the top and bottom panels, respectively. At 25 nA, with the gate voltage near the center of the plateau, the resistivity nearly vanishes and the measurements approach the noise floor. All error bars show the standard uncertainty and are omitted when they are

TRIAL MODE - Click here for more information

increased past a critical value, a breakdown of the quantized state was induced, and this effect was attributed to electron heating in parallel bulk current flow. Their work furthered the understanding of TIs by gaining a comprehension of the mechanism during the prebreakdown regime, including evidence for bulk dissipation, thermal activation and possible variable-range hopping. A concurrently reported work by Gotz et al. also looked to present a metrologically comprehensive measurement of a TI system (V-doped $(Bi,Sb)_2Te_3$) in zero magnetic field (Götz et al. 2018). When they measured the deviation of the quantized anomalous Hall resistance from R_K, they determined a value of 0.176 ± 0.25 μΩ/Ω. An example of their data is shown in Fig. 15c. The steps both works made are vital to our eventual realization of a zero-field quantum resistance standard.

One of the remaining major limitations, besides finding a TI material system with a large band gap, will be to lift the stringent temperature requirements, which are currently in the 10 mK to 100 mK range. Fijalkowski et al. show, through a careful analysis of non-local voltages in devices having a Corbino geometry, that the chiral edge channels closely tied to the observation of the QAHE continue to exist without applied magnetic field up to the Curie temperature (≈20 K) of bulk ferromagnetism in their TI system. Furthermore, it was found that thermally activated bulk conductance was responsible for quantization breakdown (Fijalkowski et al. 2021). The results give hope that one may utilize the topological protection of TI edge channels for developing a standard, as has been demonstrated most recently by Okazaki et al. (2021). They demonstrate a precision of 10 nΩ/Ω of the Hall resistance quantization in the QAHE. They directly compared both the QAHE and QHE from a conventional device to confirm their observations. Given this very recent development, more efforts are expected to follow to verify the viability of TIs as a primary standard for resistance. In the ideal case scenario, TI-based QHR devices will make disseminating the ohm more economical and portable, and will, more importantly, serve as a basis for a compact quantum ampere.

Outlook

As the global implementation of new technologies continues to progress, one should hope to see a more universal accessibility to the quantum SI. This chapter has given historical context for the role of the QHE in metrology, including a basic overview of the QHE, supporting technologies, and how metrology research has expanded these capabilities. The present-day graphene era was summarized in terms of how the new

Fig. 15 (continued) smaller than the data point. Reprinted figure with permission from (Fox et al. 2018). Copyright 2018 by the American Physical Society. (**c**) Another series of measurements on a topological insulator at the $\nu = 1$ plateau. Measurement currents of 5 nA and 10 nA were used in both orthogonal and diagonal configurations. The colored rectangles represent the weighted average and standard deviation of the data from those configurations. (Reprinted from (Götz et al. 2018), with the permission of AIP Publishing)

Uncorrected Proof

TRIAL MODE - Click here for more information

2D material performed compared with GaAs-based QHR devices, how the world began to implement it as a resistance standard, and how the corresponding measurement infrastructure has adapted to the new standard. In the third section, emerging technologies based on graphene were introduced to give a brief overview of the possible expansion of QHR device capabilities. These ideas and research avenues include *pn*J devices, QHARS devices, and experimental components of AC metrology and the quantum ampere. The chapter then concludes by discussing the possible limitations of graphene-based technology for resistance metrology and looks to explore TIs as one potential candidate to, at the very least, supplement graphene-based QHR devices for resistance and electrical current metrology.

It has become evident throughout the last few decades that the quantum Hall effect, as exhibited by our modern 2D systems both with and without magnetic fields, has the marvelous potential to unify the components of Ohm's $V = IR$ relation. That is, to bring together all three electrical quantities allowing several traceability capabilities will undoubtedly improve electrical metrology worldwide. Throughout all the coming advancements, it will be important to remember that these milestones should keep us motivated to continue learning how to better enrich society with the quantum Hall effect: AU5 AU6

> It is characteristic of fundamental discoveries, of great achievements of intellect, that they retain an undiminished power upon the imagination of the thinker. – Nikola Tesla, 1891, New York City, New York

Acknowledgments The authors wish to acknowledge S. Mhatre, A. Levy, G. Fitzpatrick, and E. Benck for their efforts and assistance during the internal review process at NIST. Commercial equipment, instruments, and materials are identified in this paper in order to specify the experimental procedure adequately. Such identification is not intended to imply recommendation or endorsement by the National Institute of Standards and Technology or the United States government, nor is it intended to imply that the materials or equipment identified are necessarily the best available for the purpose.

References AU7

Ahlers FJ, Jeanneret B, Overney F, Schurr J, Wood BM (2009) Metrologia 46:R1
Brun-Picard J, Djordjevic S, Leprat D, Schopfer F, Poirier W (2016) Phys Rev X 6:041051
Bykov AA, Zhang JQ, Vitkalov S, Kalagin AK, Bakarov AK (2005) Phys Rev B 72:245307
Cabiati F, Callegaro L, Cassiago C, D'Elia V, Reedtz GM (1999) IEEE Trans Instrum Meas 48: 314–318
Cage ME, Dziuba RF, Field BF (1985) IEEE Trans Instrum Meas 2:301–303
Cage ME, Dziuba RF, Elmquist RE, Field BF, Jones GR, Olsen PT, Phillips WD, Shields JQ, Steiner RL, Taylor BN, Williams ER (1989) IEEE Trans Instrum Meas 38:284
Clothier WK (1965) Metrologia 1:36
Cutkosky RD (1974) IEEE Trans Instrum Meas 23:305–309
De Heer WA, Berger C, Wu X, First PN, Conrad EH, Li X, Li T, Sprinkle M, Hass J, Sadowski ML, Potemski M (2007) Solid State Commun 143:92–100
Delahaye F (1993) J Appl Phys 73:7914–7920
Delahaye F, Jeckelmann B (2003) Metrologia 40:217

Uncorrected Proof

TRIAL MODE - Click here for more information

Delahaye F, Dominguez D, Alexandre F, André JP, Hirtz JP, Razeghi M (1986) Metrologia 22: 103–110

Drung D, Götz M, Pesel E, Storm JH, Aßmann C, Peters M, Schurig T (2009) Supercond Sci Technol 22:114004

Fijalkowski KM, Liu N, Mandal P, Schreyeck S, Brunner K, Gould C, Molenkamp LW (2021) Nat Commun 2021(12):1–7

Fox EJ, Rosen IT, Yang Y, Jones GR, Elmquist RE, Kou X, Pan L, Wang KL, Goldhaber-Gordon D (2018) Phys Rev B 98:075145

Giblin SP, Kataoka M, Fletcher JD, See P, Janssen TJ, Griffiths JP, Jones GA, Farrer I, Ritchie DA (2012) Nat Commun 2012(3):1–6

Giesbers AJ, Rietveld G, Houtzager E, Zeitler U, Yang R, Novoselov KS, Geim AK, Maan JC (2008) Appl Phys Lett 93:222109–222112

Götz M, Drung D, Pesel E, Barthelmess HJ, Hinnrichs C, Aßmann C, Peters M, Scherer H, Schumacher B, Schurig T (2009) IEEE Trans Instrum Meas 58:1176–1182

Götz M, Fijalkowski KM, Pesel E, Hartl M, Schreyeck S, Winnerlein M, Grauer S, Scherer H, Brunner K, Gould C, Ahlers FJ (2018) Appl Phys Lett 112:072102

Grohmann K, Hahlbohm HD, Lübbig H, Ramin H (1974) *Cryogenics* 14:499

Hamon BV (1954) J Sci Instrum 31:450–453

Hartland A (1992) Metrologia 29:175

Hartland A, Davis GJ, Wood DR (1985) IEEE Trans Instrum Meas IM-34:309

Hartland A, Jones K, Williams JM, Gallagher BL, Galloway T (1991) Phys Rev Lett 66:969–973

Hartland A, Kibble BP, Rodgers PJ, Bohacek J (1995) IEEE Trans Instrum Meas 44:245–248

He H, Kim KH, Danilov A, Montemurro D, Yu L, Park YW, Lombardi F, Bauch T, Moth-Poulsen K, Iakimov T, Yakimova R (2018) Nat Commun 9:3956

He H, Cedergren K, Shetty N, Lara-Avila S, Kubatkin S, Bergsten T, Eklund G (2021) *arXiv* preprint arXiv:2111.08280

Hu J, Rigosi AF, Kruskopf M, Yang Y, Wu BY, Tian J, Panna AR, Lee HY, Payagala SU, Jones GR, Kraft ME, Jarrett DG, Watanabe K, Takashi T, Elmquist RE, Newell DB (2018a) Sci Rep 8:15018

Hu J, Rigosi AF, Lee JU, Lee HY, Yang Y, Liu CI, Elmquist RE, Newell DB (2018b) Phys Rev B 98:045412

Hu IF, Panna AR, Rigosi AF, Kruskopf M, Patel DK, Liu CI, Saha D, Payagala SU, Newell DB, Jarrett DG, Liang CT, Elmquist RE (2021) Phys Rev B 104:085418

Jabakhanji B, Michon A, Consejo C, Desrat W, Portail M, Tiberj A, Paillet M, Zahab A, Cheynis F, Lafont F, Schopfer F (2014) Phys Rev B 89:085422

Janssen TJBM, Tzalenchuk A, Yakimova R, Kubatkin S, Lara-Avila S, Kopylov S, Fal'Ko VI. (2011) Phys Rev B 83:233402–233406

Janssen TJ, Williams JM, Fletcher NE, Goebel R, Tzalenchuk A, Yakimova R, Lara-Avila S, Kubatkin S, Fal'ko VI (2012) Metrologia 49:294

Janssen TJ, Rozhko S, Antonov I, Tzalenchuk A, Williams JM, Melhem Z, He H, Lara-Avila S, Kubatkin S, Yakimova R (2015) 2D Mater 2:035015

Jeckelmann B, Jeanneret B (2001) Rep Prog Phys 64:1603

Jeckelmann B, Jeanneret B, Inglis D (1997) Phys Rev B 55:13124

Kibble BP (1976) A measurement of the gyromagnetic ratio of the proton by the strong field method. In: Sanders JH, Wapstra AH (eds) Atomic masses and fundamental constants, vol 5. Plenum Press, New York, pp 545–551

Konemann J, Ahlers FJ, Pesel E, Pierz K, Schumacher HW (2011) IEEE Trans Instrum Meas 60: 2512–2516

Koppinen PJ, Stewart MD, Zimmerman NM (2012) IEEE Trans Electron Devices 60:78–83

Kruskopf M, Pakdehi DM, Pierz K, Wundrack S, Stosch R, Dziomba T, Götz M, Baringhaus J, Aprojanz J, Tegenkamp C, Lidzba J (2016) 2D Mater 3:041002

Kruskopf M, Rigosi AF, Panna AR, Marzano M, Patel DK, Jin H, Newell DB, Elmquist RE (2019a) Metrologia 56:065002

Uncorrected Proof

TRIAL MODE - Click here for more information

Kruskopf M, Rigosi AF, Panna AR, Patel DK, Jin H, Marzano M, Newell DB, Elmquist RE (2019b) IEEE Trans Electron Devices 66:3973–3977

Kruskopf M, Bauer S, Pimsut Y, Chatterjee A, Patel DK, Rigosi AF, Elmquist RE, Pierz K, Pesel E, Götz M, Schurr J (2021) IEEE Trans Electron Devices 68:3672–3677

Lafont F, Ribeiro-Palau R, Kazazis D, Michon A, Couturaud O, Consejo C, Chassagne T, Zielinski M, Portail M, Jouault B, Schopfer F (2015) Nat Commun 6:6806

Lara-Avila S, Moth-Poulsen K, Yakimova R, Bjørnholm T, Fal'ko V, Tzalenchuk A, Kubatkin S (2011) Adv Mater 23 878–882

Lüönd F, Kalmbach CC, Overney F, Schurr J, Jeanneret B, Müller A, Kruskopf M, Pierz K, Ahlers F (2017) IEEE Trans Instrum Meas 66:1459–1466

MacMartin MP, Kusters NL (1996) IEEE Trans Instrum Meas 15:212–220

Momtaz ZS, Heun S, Biasiol G, Roddaro S (2020) Phys Rev Appl 14:024059

Novoselov KS, Geim AK, Morozov S, Jiang D, Katsnelson M, Grigorieva I, Dubonos S, Firsov AA (2005) Nature 438:197

Novoselov KS, Jiang Z, Zhang Y, Morozov SV, Stormer HL, Zeitler U, Maan JC, Boebinger GS, Kim P, Geim AK (2007) Science 315:1379

Oe T, Matsuhiro K, Itatani T, Gorwadkar S, Kiryu S, Kaneko NH (2013) IEEE Trans Instrum Meas 62:1755–1759

Oe T, Rigosi AF, Kruskopf M, Wu BY, Lee HY, Yang Y, Elmquist RE, Kaneko N, Jarrett DG (2019) IEEE Trans Instrum Meas 2019(69):3103–3108

Okazaki Y, Oe T, Kawamura M, Yoshimi R, Nakamura S, Takada S, Mogi M, Takahashi KS, Tsukazaki A, Kawasaki M, Tokura Y (2021) Nat Phys 13:1–5

Ortolano M, Abrate M, Callegaro L (2014) Metrologia 52:31

Park J, Kim WS, Chae DH (2020) Appl Phys Lett 116:093102

Pekola JP, Saira OP, Maisi VF, Kemppinen A, Möttönen M, Pashkin YA, Averin DV (2013) Rev Mod Phys 85:1421

Poirier W, Bounouh A, Piquemal F, André JP (2004) Metrologia 41:285

Riedl C, Coletti C, Starke U (2010) J Phys D 43:374009

Rigosi AF, Glavin NR, Liu CI, Yang Y, Obrzut J, Hill HM, Hu J, Lee H-Y, Hight Walker AR, Richter CA, Elmquist RE, Newell DB (2017) Small 13:1700452

Rigosi AF, Liu CI, Wu BY, Lee HY, Kruskopf M, Yang Y, Hill HM, Hu J, Bittle EG, Obrzut J, Walker AR (2018) Microelectron Eng 194:51–55

Rigosi AF, Panna AR, Payagala SU, Kruskopf M, Kraft ME, Jones GR, Wu BY, Lee HY, Yang Y, Hu J, Jarrett DG, Newell DB, Elmquist RE (2019a) IEEE Trans Instrum Meas 68:1870–1878

Rigosi AF, Kruskopf M, Hill HM, Jin H, Wu BY, Johnson PE, Zhang S, Berilla M, Walker AR, Hacker CA, Newell DB (2019b) Carbon 142:468–474

Rigosi AF, Patel DK, Marzano M, Kruskopf M, Hill HM, Jin H, Hu J, Hight Walker AR, Ortolano M, Callegaro L, Liang CT, Newell DB (2019c) Carbon 154:230–237

Rigosi AF, Marzano M, Levy A, Hill HM, Patel DK, Kruskopf M, Jin H, Elmquist RE, Newell DB (2020) Phys B Condens Matter 582:411971

Satrapinski A, Novikov S, Lebedeva N (2013) Appl Phys Lett 103:173509

Schlamminger S, Haddad D (2019) C R Physique 20:55–63

Small GW, Ricketts BW, Coogan PC (1989) IEEE Trans Instrum Meas 38:245

Sullivan DB, Dziuba RF (1974) Rev Sci Instrum 45:517

Taylor BN (1990) IEEE Trans Instrum Meas 39:2–5

Thompson AM, Lampard DG (1956) Nature 177:888

Tiesinga E, Mohr PJ, Newell DB, Taylor BN (2021) J Phys Chem Ref Data 50:033105

Tsui DC, Gossard AC (1981) Appl Phys Lett 38:550

Tzalenchuk A, Lara-Avila S, Kalaboukhov A, Paolillo S, Syväjärvi M, Yakimova R, Kazakova O, Janssen TJ, Fal'Ko V, Kubatkin S (2010) Nat Nanotechnol 5:186–189

Von Klitzing K, Ebert G (1985) Application of the quantum Hall effect in metrology. Metrologia 21(1):11

Von Klitzing K, Dorda G, Pepper M (1980) Phys Rev Lett 45:494

Uncorrected Proof

TRIAL MODE - Click here for more information

Waldmann D, Jobst J, Speck F, Seyller T, Krieger M, Weber HB (2011) Nat Mater 10:357–360
Williams JMIET (2011) Sci Meas Technol 5:211–224
Williams JM, Janssen TJBM, Rietveld G, Houtzager E (2010) Metrologia 47:167–174
Witt TJ (1998) Rev Sci Instrum 69:2823–2843
Wood HM, Inglis AD, Côté M (1997) IEEE Trans Instrum Meas 46:269–272
Woszczyna M, Friedemann M, Dziomba T, Weimann T, Ahlers FJ (2011) Appl Phys Lett 99:022112
Woszczyna M, Friedemann M, Götz M, Pesel E, Pierz K, Weimann T, Ahlers FJ (2012) Appl Phys Lett 100:164106
Zhang N (2006) Metrologia 43:S276–S281
Zhang Y, Tan YW, Stormer HL, Kim P (2005) Nature 438:201

Uncorrected Proof

TRIAL MODE - Click here for more information

Index Terms:

Uncorrected Proof

TRIAL MODE - Click here for more information

Uncorrected Proof

TRIAL MODE - Click here for more information